Journal of Alloys and Compounds 488 (2009) 541–545

Contents lists available at ScienceDirect

Journal of Alloys and Compounds

journal homepage: www.elsevier.com/locate/jallcom

Phase transition of the orthorhombic fluorite-related compounds Ln_3IrO_7 (Ln = Pr, Nd, Sm, Eu)

Yukio Hinatsu[a,*], Yoshihiro Doi[a], Hiroaki Nishimine[a], Makoto Wakeshima[a], Mineo Sato[b]

[a] Division of Chemistry, Graduate School of Science, Hokkaido University, Sapporo 060-0810, Japan
[b] Department of Chemistry and Chemical Engineering, Faculty of Engineering, Niigata University, 8050 Ikarashi 2-nocho, Niigata 950-2181, Japan

ARTICLE INFO

Article history:
Received 2 June 2008
Received in revised form 7 October 2008
Accepted 14 October 2008
Available online 26 November 2008

Keywords:
Magnetically ordered materials
Powder metallurgy
X-ray diffraction
Heat capacity
Thermal analysis

ABSTRACT

Rare earth iridium oxides Ln_3IrO_7 (Ln = Pr, Nd, Sm, and Eu) were prepared and their structures were determined by X-ray diffraction measurements. At room temperature, Pr_3IrO_7 crystallized in an orthorhombic superstructure of cubic fluorite with space group *Cmcm*. The differential thermal analysis (DTA) and specific heat measurements for Ln_3IrO_7 (Ln = Pr, Nd, Sm, and Eu) showed a phase transition at 262, 342, 420, and 485 K, respectively. At low temperatures, Ln_3IrO_7 crystallized in a monoclinic structure with the space group $P2_1/n$. The transition temperatures increased with decreasing the ionic radius of rare earths, which indicates that the transition is stress-induced and occurs with the lattice contraction on cooling. These results for Ln_3IrO_7 were compared with the phase transitions observed for Ln_3MoO_7, Ln_3RuO_7, Ln_3ReO_7, and Ln_3OsO_7.

1. Introduction

Among rare earth elements, cerium, praseodymium, and terbium in the tetravalent state form a dioxides MO_2 with a fluorite structure. Although the trivalent rare earth does not form a dioxide with the fluorite structure, ternary rare earth oxides of the general formula Ln_3MO_7 (Ln = rare earths, M = Nb, Ru, Ta, Re, etc.) have a defect-fluorite structure. The relationship to the fluorite structure is as follows. The fluorite unit cell for oxides has the composition $M^{4+}{}_4O_8$. If the four tetravalent metal ions are replaced by three trivalent ions (Ln) and one pentavalent ion (M), one oxide-vacancy is formed per fluorite cell. Due to the significant differences in radii between the Ln^{3+} and M^{5+} ions, cation ordering occurs on the metal sites and the oxide-vacancy orders on the anion sites. In 1979, Rossell first determined the crystal structure for La_3NbO_7 [1]. It is well described in the orthorhombic space group *Cmcm*: The M^{5+} ion is coordinated with six oxygen ions, forming a MO_6 octahedron. These octahedra share corners forming one-dimensional chains which are oriented along the *c*-axis. The same space group *Cmcm* has been applied for Ln_3RuO_7 (Ln = La–Gd) [2–13], Ln_3ReO_7 (Ln = Pr, Nd, Sm–Tb) [14–17], Ln_3OsO_7 (Ln = Pr, Nd, Sm–Gd) [11,18,19], Ln_3TaO_7 (Ln = La–Nd) [20–24], Ln_3IrO_7 (Ln = Pr, Nd, Sm, Eu) [25,26], Pr_3NbO_7 [23] and Pr_3SbO_7 [23]. For Ln_3TaO_7 (Ln = Y, Sm–Ho) [20–22,24], Ln_3SbO_7 (Ln = Y, Dy, Ho) [20,27], Ln_3ReO_7 (Ln = Dy, Ho) [16,17], and Gd_3NbO_7 [20], the space group $C222_1$ has been applied. On the other hand, the structure for Ln_3MoO_7 (Ln = La–Nd, Sm, Eu) is well described with different space group $P2_12_12_1$ [28–30], and the one-dimensional MO_6 alignment is the same for the structures with the space groups *Cmcm* and $C222_1$, but the zig-zag chains of the corner-sharing MO_6 octahedra are parallel to the *b*-axis in this case.

Due to this unique crystal structures and possible related magnetic properties, many studies have been performed, especially for the magnetic properties of compounds containing Ru^{5+} ion at the *M*-site because of its largest possible spin ($S = 3/2$) [2–12].

Another topic for Ln_3MO_7 is that detailed magnetic and thermal investigations on the ruthenium-, iridium- and osmium-containing members of the Ln_3MO_7 family show low-temperature structural phase transitions [8–10,12,13,19,26,30]. However, the low-temperature structures are, in most cases, not known, or different structures were presented for the same compounds [9,12,13].

As for Ln_3IrO_7 compounds, Vente and IJdo reported the synthesis and their crystal structures [25]. They reported that Ln_3IrO_7 (Ln = Pr, Nd, Sm, and Eu) compounds are isomorphous, and their structures were described with the same space group *Cmcm*. Our X-ray diffraction and neutron diffraction measurements showed that only the structure for Pr_3IrO_7 is actually applied for such space group, and the other compounds were not the case [26]. The results for the specific heat and differential thermal analysis (DTA) indicated that

* Corresponding author. Tel.: +81 11 706 2702; fax: +81 11 706 2702.
E-mail address: hinatsu@sci.hokudai.ac.jp (Y. Hinatsu).

0925-8388/$ – see front matter © 2008 Elsevier B.V. All rights reserved.
doi:10.1016/j.jallcom.2008.10.044

the phase transitions have been observed for any of these Ln_3IrO_7 (Ln = Pr, Nd, Sm, and Eu) compounds. The high-temperature structure is well described with the space group *Cmcm*. However, the low-temperature structure has not yet been known. Concerning the magnetic properties, only the Nd_3IrO_7 showed an antiferromagnetic transition at 2.6 K [26].

In this study, we re-examined the structure and thermal properties for the Ln_3IrO_7 compounds. After checking the existence of the phase transition in these compounds, we performed the X-ray diffraction measurements in order to determine their low-temperature crystal structures. The relationship between the high- and low-temperature structures was discussed.

2. Experimental

As starting materials, rare earth oxides Ln_2O_3 (Ln = Nd, Sm, Eu) and Pr_6O_{11}, and iridium metal powders Ir were used. They were weighed in an appropriate metal ratio and were ground in an agate mortar. The mixtures were pressed into pellets and then heated in an oxygen atmosphere up to 1473–1523 K at a rate of 0.5 K min^{-1}, held at this temperature for 12 h, and then cooled down to room temperature at the same rate. After several intermediate regrindings and repelletizing, this heating procedure was repeated again. The heating in an oxygen atmosphere was necessary to avoid the formation of pyrocholore-type compounds $Ln_2Ir_2O_7$ (Ln = Pr, Nd, Sm, and Eu) in which the Ir^{4+} ions are present [31].

Powder X-ray diffraction profiles were measured using a Rigaku Multi-Flex diffractometer with Cu-Kα radiation equipped with a curved graphite monochromator. The data were collected by step-scanning in the angle range of $10^\circ \le 2\theta \le 120^\circ$ at a 2θ step-size of 0.02°. The X-ray diffraction data were analyzed by the Rietveld technique, using the programs RIETAN2000 [32].

Specific heat measurements for Ln_3IrO_7 were performed using a relaxation technique by a commercial heat capacity measuring system (Quantum Design, PPMS) in the temperature range of 1.8–400 K. The sintered sample in the form of a pellet was mounted on a thin alumina plate with Apiezon for better thermal contact.

DTA measurements were performed with a TG-DTA 2000S (Mac Science) over the temperature range of 300–800 K. As a standard material, α-Al_2O_3 was used and the rates of heating and cooling were both controlled at 10 K min^{-1}.

3. Results and discussion

3.1. Preparation and crystal structure

We have successfully prepared a series of compounds Ln_3IrO_7 (Ln = Pr, Nd, Sm, Eu) in an oxygen atmosphere. Fig. 1 shows their X-ray diffraction (XRD) profiles measured at 298 K and the fitting results by the Rietveld analysis. Vente et al. reported that the crystal structures for Ln_3IrO_7 (Ln = Pr, Nd, Sm, Eu) were orthorhombic with space group *Cmcm*. Following them, we also refined the structures with the same space group. The fitting results by the Rietveld analysis shown in Fig. 1 appear to indicate that the structures for Ln_3IrO_7 (Ln = Pr, Nd, Sm, Eu) were refined with the space group *Cmcm* and the goodness of the fit (S) [32] was below 1.30 for all the compounds. However, the detailed X-ray diffraction profiles in the low 2θ angles (the inset of Fig. 1) indicate that some additional diffraction lines which cannot be fitted with the *Cmcm* space group appeared at $2\theta \sim 22^\circ$ and 25° for Ln_3IrO_7 (Ln = Nd, Sm, Eu).

Fig. 2 shows the temperature dependence of the specific heat for Pr_3IrO_7 and Nd_3IrO_7. Specific heat anomalies corresponding to the first-order phase transitions were observed at 261 K and 342 K for Pr_3IrO_7 and Nd_3IrO_7, respectively. For Sm_3IrO_7 and Eu_3IrO_7, corresponding anomalies were observed in the DTA measurements, i.e., the endothermic peaks during heating were found at 420 K for Sm_3IrO_7 and 485 K for Eu_3IrO_7. We consider that this transition is due to the phase transition. The transition temperature (T_p) increased with decreasing Ln ionic radius (Pr → Eu). Only the Pr_3IrO_7 has a high-temperature structure at room temperature (T_p = 261 K). Therefore, Nd_3IrO_7, Sm_3IrO_7 and Eu_3IrO_7 should show a phase transition when the temperature is increased above room temperature.

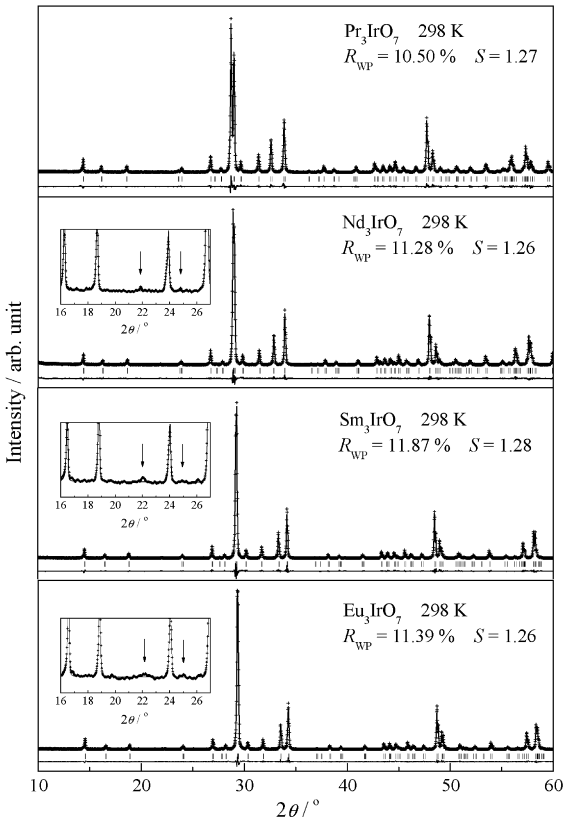

Fig. 1. Powder X-ray diffraction profiles for Ln_3IrO_7 (Ln = Pr, Nd, Sm, Eu) measured at 298 K. The calculated and observed profiles are shown on the top solid line and cross-markers, respectively. The vertical marks in the middle show positions calculated for Bragg reflections. The lower trace is a plot of the difference between calculated and observed intensities. The insets show the X-ray diffraction profiles measured for Nd_3IrO_7, Sm_3IrO_7, and Eu_3IrO_7 in the $12^\circ \le 2\theta \le 28^\circ$. Arrows show diffraction lines which cannot be assigned with the space group *Cmcm*.

We performed high-temperature XRD measurements for Nd_3IrO_7 in the temperature range of 298–550 K. Fig. 3 shows the XRD profiles in the low 2θ range measured at 298 and 400 K. The XRD profile measured at 298 K has some weak diffraction lines (for example, at $2\theta \sim 22^\circ$ and 25°) which cannot be assigned with space group *Cmcm*. When the temperature was increased above 342 K, such diffraction lines disappeared and the XRD profile was successfully refined with the space group *Cmcm*. The same situation was observed in the temperature dependence of the XRD profiles for

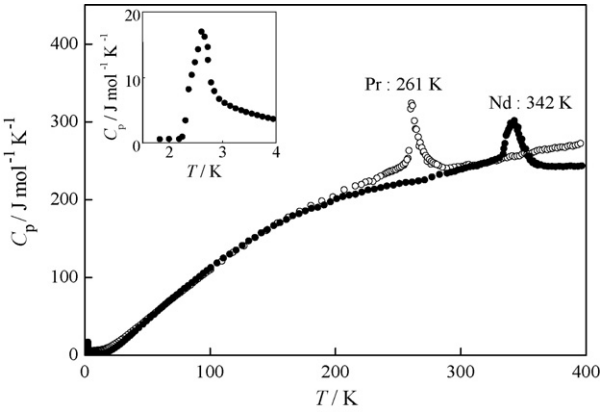

Fig. 2. Temperature dependence of the specific heat for Pr_3IrO_7 and Nd_3IrO_7. The inset shows the detailed specific data for Nd_3IrO_7 at low temperatures.

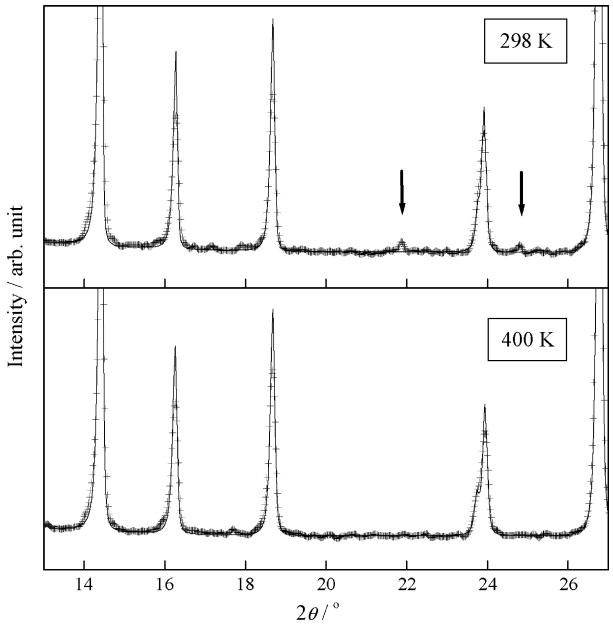

Fig. 3. XRD profiles for Nd_3IrO_7 measured at 298 and 400 K in the 2θ range of 13–27°. Diffraction lines marked with arrows disappeared when the temperature is raised up to 400 K.

Sm_3IrO_7 and Eu_3IrO_7. The high-temperature structure for Ln_3IrO_7 is well described with the space group *Cmcm*, and this structure has been observed for most of the Ln_3MO_7 type compounds [2–27].

The analysis of the X-ray diffraction data measured below the transition temperature showed that all additional diffraction peaks could be indexed to a primitive monoclinic cell. Refinement in the $P2_1/n$ space group of the structural model yielded satisfactory results. Trial refinements in other space groups resulted in physically unreasonable displacement parameters, as well as high residual factors *R*. The refined atomic coordinates and lattice parameters for the low-temperature structure of Nd_3IrO_7 with those for the high-temperature structure are compiled in Table 1. The high-temperature structure is described in the orthorhombic space group *Cmcm* with two independent neodymium positions ($Nd1_o$, $Nd2_o$, where the subscript "o" means orthorhombic), one unique iridium site ($Ir1_o$), and three independent oxygen atom positions ($O1_o$, $O2_o$, $O3_o$). The low-temperature structures are best described in the primitive monoclinic space group $P2_1/n$ with three independent neodymium positions, two unique iridium sites, and seven independent oxygen atom positions. Due to this transition (orthorhombic → monoclinic), $Ir1_o$ transforms into $Ir1_m$ and $Ir2_m$ (where the subscript "m" means monoclinic), $Nd1_o$ transforms into $Nd1_m$, $Nd2_o$ transforms into $Nd2_m$ and $Nd3_m$. As for oxygen atoms, $O1_o$, $O2_o$, and $O3_o$ transform into ($O2_m$, $O3_m$, $O4_m$ and $O5_m$), ($O6_m$ and $O7_m$), and $O1_m$, respectively.

Fig. 4 shows the low-temperature structure of Nd_3IrO_7 as well as its high-temperature structure. Similar to the high-temperature structure, the structure features chains of vertex-shared IrO_6 octahedra running along the *c*-axis. In the high-temperature *Cmcm* structure (Fig. 4(a)), the chains of trans vertex-sharing IrO_6 connect to the chains of edge-sharing NdO_8 pseudo-cubes via pairs of equatorial IrO_6 oxygen atoms. In the low-temperature $P2_1/n$ structure (Fig. 4(b)), the vertex-shared IrO_6 octahedra are tilted greatly. The tilting of the IrO_6 chains caused one of the equatorial oxygen atoms to rotate away from the neodymium cation. This resulted in the reduction of the coordination number of the associated Nd^{3+} from 8 to 7. The Nd–O bond length 2.75 Å which is included in the NdO_8 pseudo-cube at 400 K ($Nd1_o$–$O1_o$ with space group *Cmcm*) extends to 3.11 Å at 298 K ($Nd1_m$–$O2_m$ with space group $P2_1/n$). The $O2_m$ at a distance of 3.11 Å from the Nd1 does not form the coordination polyhedron. This oxygen shift is the most remarkable change through the phase transition, and it corresponds to a dramatic change of the lattice parameters against the temperature. We measured the temperature dependence of the lattice parameters for Nd_3IrO_7 [26], and it is shown in Fig. 5. In the case that the lattice parameters were refined with the same space group *Cmcm*, they changed drastically near 342 K, at which the specific heat anomaly was observed. When the temperature was decreased through 342 K, the lattice parameter *b* was found to increase, while the lattice parameters *a* and *c* decreased rapidly. It should be noted that the IrO_6 octahedra

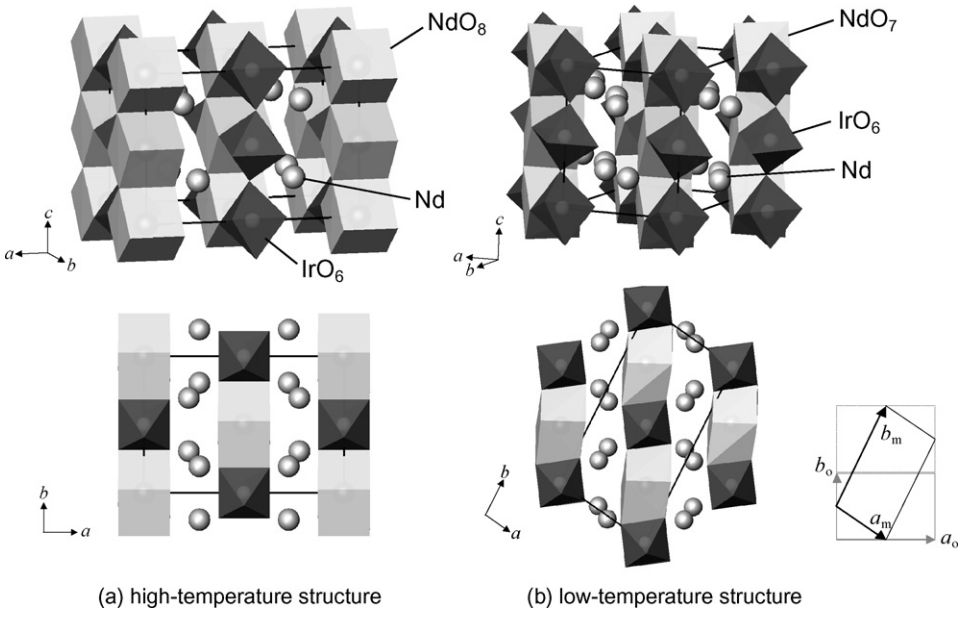

Fig. 4. Crystal structures of Nd_3IrO_7. (a) High-temperature structure, *Cmcm*; (b): low-temperature structure, $P2_1/n$. The relationship between the monoclinic unit cell (the low-temperature structure) and the orthorhombic unit cell (the high-temperature structure) is also indicated.

Table 1
Crystal structure data for Nd_3IrO_7.

Site		x	y	z	B/Å^2
High-temperature structure (400 K)					
Space group: *Cmcm*					
a = 10.8991(1) Å, b = 7.4464(7) Å, c = 7.4930(8) Å, V = 608.12(10) Å^3					
R_I = 2.37%, R_{wp} = 12.10%					
Nd1	4*a*	0	0	0	0.99(2)
Nd2	8*g*	0.2234(2)	0.3051(2)	1/4	0.99
Ir	4*b*	0	1/2	0	0.29(5)
O1	16*h*	0.1286(8)	0.3150(3)	0.9580(7)	0.815(2)
O2	8*g*	0.1314(9)	0.0243(1)	1/4	0.5(1)
O3	4*c*	0	0.4066(2)	1/4	0.5
Low-temperature structure (298 K)					
Space group: $P2_1/n$					
a = 6.6024(7) Å, b = 12.4268(1) Å, c = 7.4938(6) Å, γ = 98.35°, V = 608.32(10) Å^3					
R_I = 2.01%, R_{wp} = 11.73%					
Nd1	4*e*	0.2340(4)	0.7577(5)	−0.0022(2)	0.63(7)
Nd2	4*e*	0.4318(5)	0.0141(2)	0.2521(2)	0.63
Nd3	4*e*	0.7618(6)	0.7914(5)	0.2521(3)	0.63
Ir1	2*a*	0	0	0	0.21(5)
Ir2	2*c*	1/2	1/2	0	0.21
O1	4*e*	0.5578(4)	0.4569(1)	0.2486(3)	0.55(5)
O2	4*e*	0.2006(2)	0.5070(1)	0.0465(1)	0.55
O3	4*e*	0.7131(5)	0.0043(1)	0.0344(1)	0.55
O4	4*e*	0.5644(4)	0.6641(1)	0.0194(1)	0.55
O5	4*e*	0.0630(1)	0.1619(1)	0.0699(1)	0.55
O6	4*e*	0.9574(5)	0.3326(1)	0.2628(2)	0.55
O7	4*e*	0.5611(4)	0.2040(1)	0.2819(3)	0.55

maintain their edge-sharing connectivity with the $Nd1O_7$ polyhedra. In the low-temperature structure, the IrO_6 chains still connect to the neodymium chains to form sheets, as shown in Fig. 4(b). The Ir–Nd–O slabs are more distorted in the low-temperature structure. The remaining two-thirds of the neodymium cations, Nd2 and Nd3, exist in two crystallographically unique sites.

On the other hand, the Ir–O distances are not affected by the phase distortion, and the average Ir–O distances are 1.97–1.98 Å for any of the Ln_3IrO_7 (*Ln* = Pr, Nd, Sm, Eu) compounds. These distances are in good agreement with lengths calculated from the Shannon's ionic radii [33].

Fig. 6 shows the variation of the phase transition temperatures for a series of Ln_3MO_7 (*M* = Mo, Ru, Re, Os, Ir) compounds against the ionic radius of Ln^{3+} [12,16,19,26,30]. For each of the five series

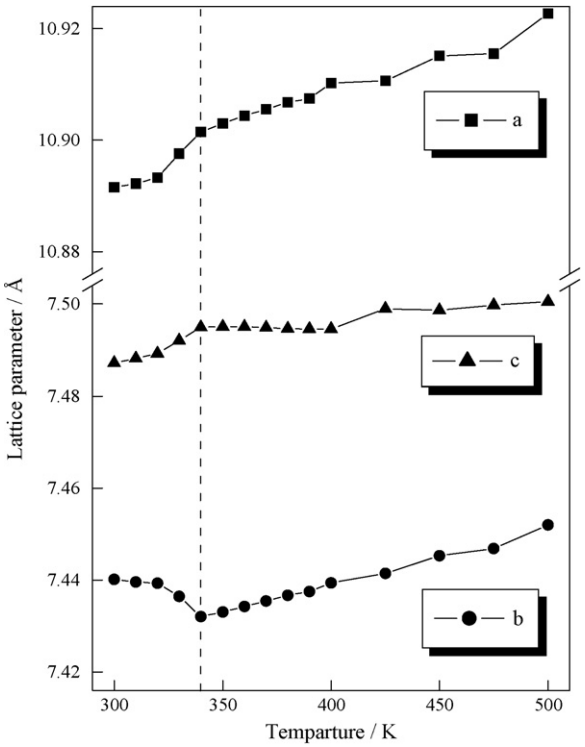

Fig. 5. Temperature dependence of lattice parameters for Nd_3IrO_7.

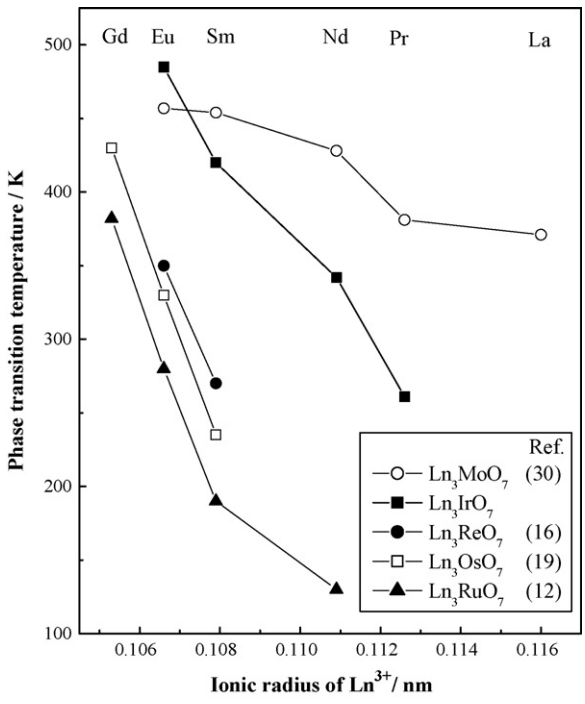

Fig. 6. Phase transition temperature for Ln_3MO_7 (*M* = Mo, Ru, Re, Os, Ir) against the ionic radius of Ln^{3+}.

of Ln_3MO_7 compounds, the phase transition temperatures decrease with increasing the ionic radius of Ln^{3+}, i.e., it has been observed that the phase transition of Ln_3MO_7 is clearly influenced by the size of the Ln^{3+} cation. The transition is stress-induced and occurs with lattice contraction on cooling. Each transition temperature within a series is separated by approximately the same temperature interval except for the case of Ln_3MoO_7. The trend of the transition temperature against Ln^{3+} radius for Ln_3MoO_7 is different from those for Ln_3MO_7 (M = Ru, Re, Os, Ir). The reason for this may be related to the difference in their high-temperature structures, that is, the Ln_3MoO_7 (Ln = La–Eu) exists in $P2_12_12_1$ structure, whereas the other Ln_3MO_7 (M = Ru, Re, Os, Ir) exists in the *Cmcm* structure.

4. Summary

Lanthanide iridates Ln_3IrO_7 (Ln = Pr, Nd, Sm, and Eu) were formed in the orthorhombic superstructure of cubic fluorite with space group *Cmcm*. These compounds show a phase transition at 262, 342, 420, and 485 K for Ln = Pr, Nd, Sm, and Eu, respectively. At low temperatures, they crystallize in a monoclinic structure with the space group $P2_1/n$. The transition temperatures increased with decreasing the ionic radius of rare earths, which indicates that the transition is stress-induced and occurs with the lattice contraction on cooling.

Acknowledgement

This work was supported by Grant-in-aid for Scientific Research, No. 20550052 from the Ministry of Education, Science, Sports and Culture of Japan.

References

[1] H.J. Rossell, J. Solid State Chem. 27 (1979) 115–122.
[2] F.P.F. van Berkel, D.J.W. IJdo, Mater. Res. Bull. 21 (1986) 1103–1106.
[3] W.A. Groen, F.P.F. van Berkel, D.J.W. IJdo, Acta Crystallogr. Sec. C 43 (1986) 2262–2264.
[4] P. Khalifah, R.W. Erwin, J.W. Lynn, Q. Huang, B. Batlogg, R.J. Cava, Phys. Rev. B 60 (1999) 9573–9578.
[5] P. Khalifah, Q. Huang, J.W. Lynn, R.W. Erwin, R.J. Cava, Mater. Res. Bull. 35 (2000) 1–7.
[6] F. Wiss, N.P. Raju, A.S. Wills, J.E. Greedan, Int. J. Inorg. Mater. 2 (2000) 53–59.
[7] B.P. Bontchev, A.J. Jacobson, M.M. Gospodinov, V. Skumryev, V.N. Popov, B. Lorenz, R.L. Meng, A.P. Litvinchuk, M.N. Iliev, Phys. Rev. B 62 (2000) 12235–12240.
[8] D. Harada, Y. Hinatsu, J. Solid State Chem. 158 (2001) 245–253.
[9] D. Harada, Y. Hinatsu, Y. Ishii, J. Phys.: Condens. Matter 13 (2001) 10825–10836.
[10] D. Harada, Y. Hinatsu, J. Solid State Chem. 164 (2002) 163–168.
[11] R. Lam, F. Wiss, J.E. Greedan, J. Solid State Chem. 167 (2002) 182–187.
[12] W.R. Gemmill, M.D. Smith, H.-C. zur Loye, Inorg. Chem. 43 (2004) 4254–4261.
[13] N. Ishizawa, K. Hiraga, D. du Boulay, H. Hibino, T. Ida, S. Oishi, Acta Cryst. E62 (2006) i13–i16.
[14] G. Wltschek, H. Paulus, I. Svoboda, H. Ehrenberg, H. Fuess, J. Solid State Chem. 125 (1996) 1–4.
[15] R. Lam, T. Langet, J.E. Greedan, J. Solid State Chem. 171 (2002) 317–323.
[16] Y. Hinatsu, M. Wakeshima, N. Kawabuchi, N. Taira, J. Alloys Compd. 374 (2004) 79–83.
[17] M. Wakeshima, Y. Hinatsu, J. Solid State Chem. 179 (2006) 3575–3581.
[18] J.R. Plaisier, R.J. Drost, D.J.W. IJdo, J. Solid State Chem. 169 (2002) 189–198.
[19] W.R. Gemmill, M.D. Smith, Y.A. Mozharivsky, G.J. Miller, H.-C. zur Loye, Inorg. Chem. 44 (2005) 7047–7055.
[20] J.G. Allpress, H.J. Rossell, J. Solid State Chem. 27 (1979) 105–114.
[21] Y. Yokogawa, M. Yoshimura, S. Somiya, Mater. Res. Bull. 22 (1987) 1449–1456.
[22] Y. Yokogawa, M. Yoshimura, S. Somiya, Solid State Ionics 28 (1988) 1250–1253.
[23] J.F. Vente, R.B. Helmholdt, D.J.W. IJdo, J. Solid State Chem. 108 (1994) 18–23.
[24] M. Wakeshima, Y. Hinatsu, J. Phys.: Condens. Matter 16 (2004) 4103–4120.
[25] J.F. Vente, D.J.W. IJdo, Mater. Res. Bull. 26 (1991) 1255–1262.
[26] H. Nishimine, M. Wakeshima, Y. Hinatsu, J. Solid State Chem. 177 (2004) 739–744.
[27] T. Fennell, S.T. Bramwell, M.A. Green, Can. J. Phys. 79 (2001) 1415–1419.
[28] J.E. Greedan, N.P. Raju, A. Wegner, P. Gougeon, J. Padiou, J. Solid State Chem. 129 (1997) 320–327.
[29] N. Barrier, P. Gougen, Acta Crystallogr. E59 (2003) i22–i24.
[30] H. Nishimine, M. Wakeshima, Y. Hinatsu, J. Solid State Chem. 178 (2005) 1221–1229.
[31] N. Taira, M. Wakeshima, Y. Hinatsu, J. Phys.: Conden. Matter 13 (2001) 5527–5534.
[32] F. Izumi, T. Ikeda, Mater. Sci. Forum 198 (2000) 321–324.
[33] R.D. Shannon, Acta Crystallogr. A32 (1976) 751–767.